

Intra-unit-cell nematic charge order in the titanium-oxypnictide family of superconductors

Benjamin A. Frandsen*,¹ Emil S. Bozin,^{2,*} Hefei Hu,² Yimei Zhu,² Yasumasa Nozaki,³ Hiroshi Kageyama,³ Yasutomo J. Uemura,¹ Wei-Guo Yin,² and Simon J. L. Billinge^{2,4,†}

¹*Department of Physics, Columbia University, New York, NY 10027, USA.*

²*Condensed Matter Physics and Materials Science Department, Brookhaven National Laboratory, Upton, NY 11973, USA.*

³*Department of Energy and Hydrocarbon Chemistry, Graduate School of Engineering, Kyoto University, Nishikyo, Kyoto 615-8510, Japan.*

⁴*Department of Applied Physics and Applied Mathematics, Columbia University, New York, NY 10027, USA.*

Understanding the role played by broken symmetry states such as charge, spin, and orbital orders in the mechanism of emergent properties such as high-temperature superconductivity (HTSC) is a major current topic in materials research. That the order may be within one unit cell, such as nematic, was only recently considered theoretically, but its observation in the iron-pnictide and doped cuprate superconductors places it at the forefront of current research. Here we show that the recently discovered $\text{BaTi}_2\text{Sb}_2\text{O}$ superconductor and its “parent” compound $\text{BaTi}_2\text{As}_2\text{O}$ form a symmetry-breaking nematic ground state that can be naturally explained as an intra-unit-cell charge order with d -wave symmetry, pointing to the ubiquity of the phenomenon. These findings, together with the key structural features in these materials being intermediate between the cuprate and iron-pnictide HTSC materials, render the titanium oxypnictides an important new material system to understand the nature of nematic order and its relationship to superconductivity.

Rather than being an anomalous side-effect in one or two cuprate systems, broken-symmetry states are now thought to be widespread in strongly correlated electron systems and other complex materials. Extensive study of the manganites^{1,2}, cuprates^{3,4}, iron pnictides⁵, and a variety of other systems has made it increasingly evident that local and global symmetry-breaking in the charge, orbital, lattice, and spin degrees of freedom are associated with the appearance of emergent phenomena such as colossal magnetoresistance and high-temperature superconductivity (HTSC), but the exact relationship is not understood. Historically, the study of such broken-symmetry states has been very challenging. Taking the cuprates as an example, eight years elapsed from the initial discovery of superconductivity to the first observation of symmetry-broken charge order (stripes) in one system⁶, another seven years passed before hints were found in others^{7,8}, and only within the last three years has charge order begun to emerge as a possibly ubiquitous feature of the cuprates^{9,10}.

Several possibilities arise when considering the symmetries that can be broken by these states. Most charge/spin-density-waves (C/SDWs) break the translational symmetry of the lattice, folding the Brillouin zone and resulting in superlattice diffraction peaks. On the other hand, orbital ordering, where charge transfers between orbitals centered at the same site, can break the metric rotational symmetry without lowering the translational symmetry. Examples are charge-nematic¹¹ and loop-current^{12,13} orders in the doped cuprates. In this context, nematic order is defined as one that breaks the rotational point group symmetry while preserving the lattice translational symmetry. The fact that nematic symmetry-broken states have recently been discovered experimentally in both the cuprate¹¹ and iron-based¹⁴

superconductors raises the importance and relevance of this observation to HTSC. It is therefore critically important to understand the role and ubiquity of symmetry breaking, including intra-unit-cell nematicity, to the superconducting phenomenon.

Standard theoretical treatments of HTSC such as the effective single-band $t - J$ model have typically ignored the possibility of intra-unit-cell orders¹⁵. When multiple atoms per unit cell are explicitly included in the theory, qualitatively different ground-state solutions may be found¹⁶, underscoring the subtlety and importance of accounting correctly for this phenomenon. Hence, finding related but distinct systems that exhibit this phenomenon is expected to shed new light on this critical question.

Very recently, superconductivity was discovered^{17–19} in titanium-oxypnictide compounds such as $\text{ATi}_2\text{Pn}_2\text{O}$ ($A = \text{Na}_2, \text{Ba}, (\text{SrF})_2, (\text{SmO})_2$; $\text{Pn} = \text{As}, \text{Sb}, \text{Bi}$), which are close structural and chemical cousins to the cuprates and iron-pnictides^{20–24}. In particular, in isovalent $\text{BaTi}_2(\text{Sb}_{1-x}\text{Bi}_x)_2\text{O}$ and aliovalent $\text{Ba}_{1-x}\text{Na}_x\text{Ti}_2\text{Sb}_2\text{O}$,²⁵ muon spin rotation and heat capacity measurements point to fully-gapped s -wave superconductivity^{26–28}. Interestingly, a number of compounds in this family also show strong anomalies in resistivity and/or magnetic susceptibility that are thought to be signatures of symmetry-breaking charge- or spin-ordered ground states^{21,24,25,29,30}, suggesting that these materials are excellent candidates for studying the interplay between broken-symmetry states and superconductivity. In light of these strong transport anomalies, it is then quite surprising that subsequent experiments have failed to uncover any direct evidence of a symmetry-lowered phase at low temperatures^{26,27,31}, leaving open the question of whether these materials do possess symmetry-

broken ground states.

Here we show that superconducting $\text{BaTi}_2\text{Sb}_2\text{O}$, and its non-superconducting “parent” compound $\text{BaTi}_2\text{As}_2\text{O}$, do indeed undergo a tetragonal-orthorhombic phase transition, corresponding to a $C_4 - C_2$ symmetry lowering, that occurs at the temperature of the transport anomaly. On the other hand, high-sensitivity electron diffraction measurements failed to detect any superlattice peaks in the bulk at low temperature, indicating that this transition does not break translational symmetry. The low-temperature phase therefore constitutes a nematic state. In light of the pronounced upturn in resistivity accompanying this nematic transition, together with the absence of any ordered SDW²⁶, we attribute the nematicity to an intra-unit-cell charge order with d -wave symmetry by charge transfer between neighboring Ti sites—similar to that between neighboring oxygen sites in cuprate superconductors—and found it naturally explains the temperature dependence of the lattice constants. These results establish this family of materials as another playground for studying symmetry-breaking electronic phases and their relationship to superconductivity.

The basic structural unit of $\text{BaTi}_2Pn_2\text{O}$ is a planar square net of titanium and oxygen, in analogy with the cuprates [Fig. 1(a) and (b)], with the crucial difference that the positions of the metal and oxygen ions are switched between the structures [the complete titanate structure is shown as an inset in Fig. 2(b)]. In Fig. 1, the square net is shown by solid lines along the nearest neighbor bonds, with dashed lines showing the net joining second neighbor ions. This second-nearest-neighbor square net connects oxygen ions in the cuprates, but metal ions in the titanate compounds and also in the iron-based superconductors [Fig. 1(c)]. Thus, in terms of chemistry and structure, the titanate compounds bridge between the ferrous and cuprate superconductors. The Ti $3d$ orbitals are occupied by one electron per Ti atom, which is found to reside in a nominally $1/4$ -filled band formed via hybridization of the d_{xy} and $d_{y^2-z^2}/d_{x^2-z^2}$ orbitals for the Ti(1)/Ti(2) ions (defined in Fig. 1(b)). The local geometry of the Ti(1) site is shown in Fig. 1(d) and the arrangement of the d -energy levels in Fig. 1(e).

Furthermore, the phase diagram [Fig. 2(b)] is highly reminiscent of the cuprates and iron-based superconductors, with superconductivity appearing on doping and transport behavior that is strongly suggestive of a competing electronic transition such as the formation of a CDW or SDW^{21,24}. The transport is metallic at high temperature²¹, with a positive resistivity slope vs. temperature [Fig. 2(a)]. However, on cooling a pronounced upturn in the resistivity is found for all x in the solid solution $\text{BaTi}_2\text{As}_{1-x}\text{Sb}_x\text{O}$. The feature occurs at a temperature T_a that decreases monotonically from 200 K for $x = 0$ to 50 K for $x = 1$, with superconductivity appearing below approximately 1 K for the antimony endmember and increasing to 5 K for $\text{BaTi}_2\text{Bi}_2\text{O}$.^{19,24} Anomalies in the magnetic susceptibility and specific heat are also observed²¹ at T_a .

Density functional theory (DFT) calculations for $\text{BaTi}_2\text{Sb}_2\text{O}$ predicted an instability towards a bicollinear SDW formation^{32,33} or a commensurate CDW ground state driven by an unstable phonon mode that doubles the unit cell by distorting the Ti squares and preserves the tetragonal symmetry³⁴. The possibility of SDW formation in $\text{BaTi}_2(\text{As,Sb})_2\text{O}$ was subsequently ruled out by muon spin relaxation and ^{121/123}Sb nuclear resonance measurements, which show conclusively that no magnetic order develops at any temperature probed^{26,27,31}. On the other hand, a conventional CDW should be evident through an associated structural distortion. However, initial electron and neutron diffraction studies on the Sb endmember²⁶ found no broken symmetry or any signature of superlattice formation at low temperatures, nor was a CDW gap formation observed in angle-resolved photoemission measurements of the nested Fermi surfaces (although a slight depression of the density of states at other momenta was found to correlate in temperature with the resistivity anomaly³⁵).

In the absence of evidence for a long-range ordered CDW, we undertook a neutron diffraction and total scattering measurement on $\text{BaTi}_2\text{Sb}_2\text{O}$ with a dense set of temperature points to search for evidence for a possible short-range ordered CDW^{36,37}. We also extended the investigation to the previously unstudied $\text{BaTi}_2\text{As}_2\text{O}$ endmember. Unexpectedly, we found a long-range structural phase transition at T_a . Room temperature measurements of $\text{BaTi}_2\text{As}_2\text{O}$ confirm the tetragonal $P4/mmm$ space group symmetry previously reported from x-ray diffraction²¹. However, on cooling through T_a we observe a distinct splitting of the (200)/(020) and (201)/(021) Bragg peaks, representing the first observation of a symmetry lowering at the same temperature as the resistivity anomaly in $\text{BaTi}_2\text{As}_2\text{O}$. This is shown in Fig. 3, which compares the high- and low-temperature Bragg peaks in panel (a) and displays their temperature evolution in panel (b). The (200) peak at 2.04 Å begins to broaden below 200 K, coinciding with T_a , and appears to split at the lowest temperatures. Similarly, the (201) peak at 1.94 Å displays apparent splitting as the temperature is lowered. These observations demonstrate that $\text{BaTi}_2\text{As}_2\text{O}$ undergoes a long-range-ordered structural phase change at T_a , lowering its symmetry from tetragonal to orthorhombic.

To investigate the structural transition in greater detail, we performed LeBail³⁸ refinements at all temperatures. We used the parent $P4/mmm$ model for $T \geq 200$ K. The simplest possible symmetry-breaking distortion mode of the parent $P4/mmm$ structure consistent with the observed peak splitting is a mode that breaks the degeneracy of the a - and b -axes without otherwise shifting atoms within the unit cell, resulting in a space-group symmetry of $Pmmm$, which was used for $T < 200$ K. We display the results of these refinements in Fig. 4. As seen in panel (b), the tetragonal a -axis clearly splits below $T \sim 200$ K, with a maximum orthorhombic splitting of approximately 0.01 Å. The orthorhombicity parameter $\eta = 2 \times (a - b)/(a + b)$ is shown in the inset

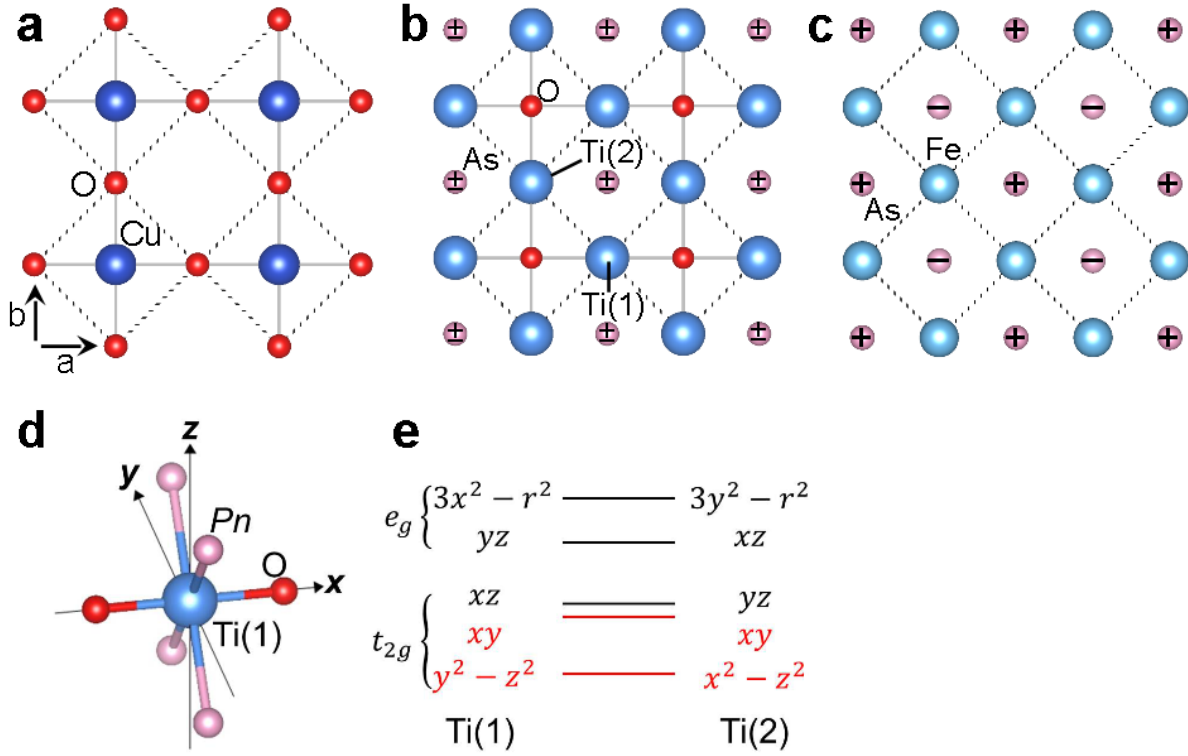


FIG. 1. Planar geometries of cuprate, titanium-oxypnictide, and iron-pnictide superconducting families. (a-c) Planar motifs in cuprates, titanium oxypnictides, and iron pnictides, respectively. Solid gray lines show the metal-anion square net, and dotted black lines show the square net of second-nearest-neighbor atoms. The + and - signs in (b) and (c) denote As atoms that are above and below the plane, respectively. (d) TiO₂Pn₄ octahedral motif found in BaTi₂Pn₂O. (e) Schematics of the Ti 3d-orbital energy levels for the two distinct Ti sites labeled in (b), Ti(1) and Ti(2). The two lowest-lying orbitals marked in red form two bands occupied by one electron per Ti.

of panel (a), indicating a maximum orthorhombicity of $\sim 0.22\%$. Panel (a) also displays the temperature dependence of the c -axis parameter, which exhibits an upturn below the structural transition deviating from the linear thermal contraction trend seen for $T > 200$ K. This same type of c -axis response also accompanies long-range ordered stripe formation in the nickelates³⁶. The superconducting BaTi₂Sb₂O shows qualitatively the same behavior, albeit with an amplitude decreased by a factor of approximately 5, with an orthorhombic splitting (0.05%) and a small but observable c -axis upturn appearing on cooling through $T_a = 50$ K. The undistorted $P4/mmm$ model can be used with moderate success at all temperatures, but the $Pmmm$ model yields a better fit below 50 K (see Supplementary Information Section 2). Further assessment including Rietveld refinements and pair distribution function analysis is consistent with these observations for both compounds and can be found in Supplementary Information Sections 1-3.

These results offer compelling evidence that the observed structural response is intimately related to the transport anomaly and may be driven by a broken symmetry of the electronic system forming at that temperature. The small distortion amplitude in BaTi₂Sb₂O explains why this long-range structural phase change

escaped notice in previous neutron diffraction measurements²⁶.

Since CDW formation is implicated, we made a special effort to search for the appearance of weak superlattice peaks associated with a finite CDW wavevector in electron-diffraction (ED) patterns below T_a . The original study on the antimony endmember failed to observe superlattice peaks²⁶. Here we concentrated on the arsenic endmember where the structural distortion is five times larger, and the ED patterns were heavily overexposed to search for any weak response at intensities close to background. Despite these efforts, the ED patterns taken along the [001] and [011] directions revealed no superlattice peaks in the bulk at low temperature, as shown in Fig. 5. However, in a very small fraction of the sample in the immediate vicinity of grain boundaries, weak superlattice peaks with $\mathbf{Q} = (1/2, 0, 0)$ are observed at low temperature. This non-bulk behaviour is explored further in Supplementary Information Section 4.

A picture emerges of a $C_4 - C_2$ symmetry breaking occurring with an accompanying strong upturn in resistivity, but with no corresponding CDW superlattice peaks appearing. The resistivity upturn is larger than would be expected as a passive response of the electronic system to

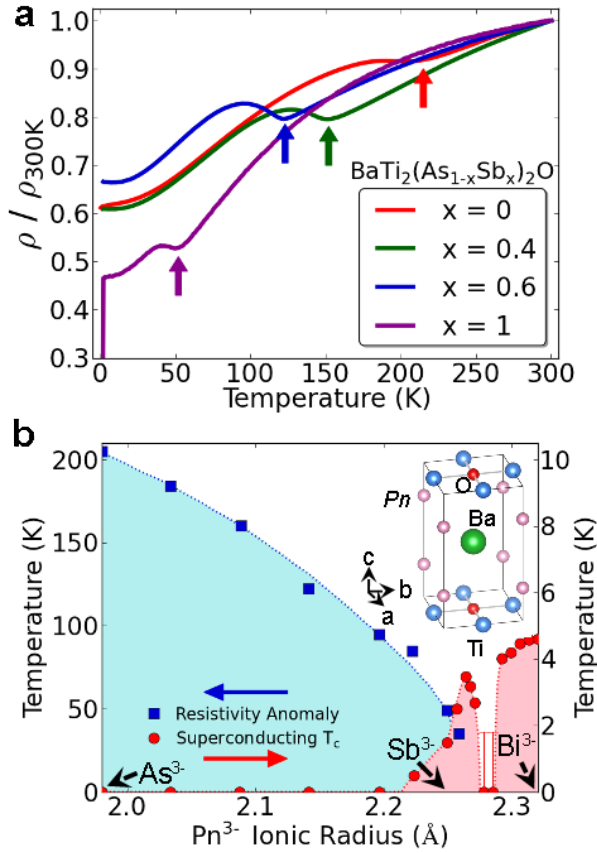


FIG. 2. Transport characteristics and phase diagram of $\text{BaTi}_2\text{Pn}_2\text{O}$ with $\text{Pn}=\text{As}, \text{Sb}, \text{Bi}$. (a) Electrical resistivity of $\text{BaTi}_2\text{As}_{1-x}\text{Sb}_x\text{O}$, normalized by the room-temperature resistivity. Arrows indicate the anomaly discussed in the text. (b) Phase diagram of $\text{BaTi}_2\text{Pn}_2\text{O}$ shown as a function of Pn^{3-} ionic diameter. Broken lines are guides to the eye. Inset: tetragonal crystal structure of $\text{BaTi}_2\text{Pn}_2\text{O}$.

the structural transition, borne out by a standard DFT calculation with the observed orthorhombicity parameter $\eta = 0.22\%$ which showed that merely 0.0003 electrons are transferred from $\text{Ti}(1)$ to $\text{Ti}(2)$. Therefore, in common with earlier discussion^{18,21}, we propose that the structural transition is a response to an instability of the electronic system. The earlier muon spin relaxation results^{26,27}, together with the ED measurements, allow us to rule out the existing proposals of SDW formation^{32,33} or a phonon-driven CDW³⁴. Instead, an intra-unit-cell charge-nematic electronic symmetry breaking is implicated, similar to that proposed for doped cuprates³⁹.

In the current case, a charge redistribution between the on-site orbital states at the Fermi level, $d_{x^2-z^2}/d_{y^2-z^2}$ to d_{xy} , does not break the rotational symmetry but does break translational symmetry, so can be ruled out. Instead, a simple but novel intra-unit-cell CDW naturally explains the observed phenomenology. A transfer of charge from $\text{Ti}(1)$ to $\text{Ti}(2)$ [see Fig. 1(b)] lowers the rotational symmetry of the Ti_2O plaquette locally from C_4 to C_2 , with the effect on the overall lat-

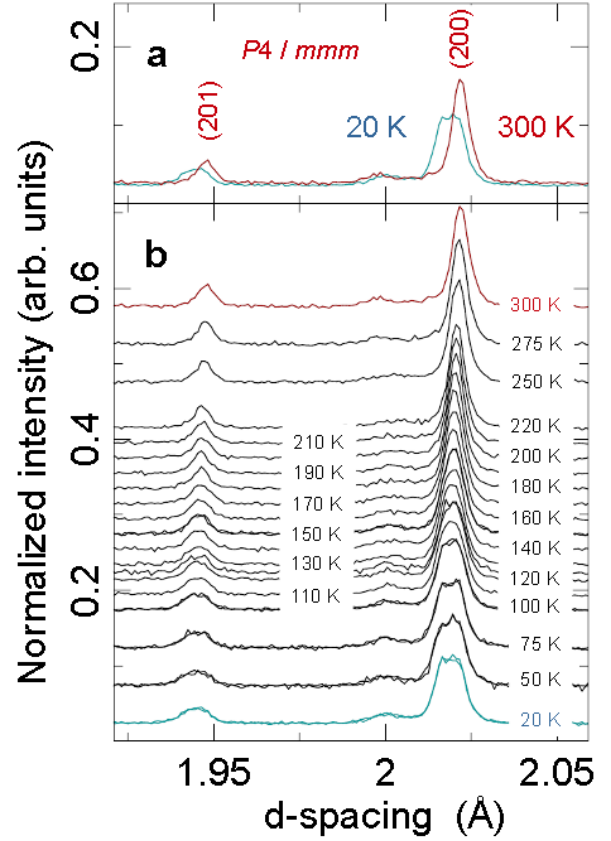


FIG. 3. Temperature evolution of $\text{BaTi}_2\text{As}_2\text{O}$ neutron diffraction pattern. (a) Comparison of normalized intensities of 300 K (red) and 20 K (blue) data around (200) and (201) reflections in $P4/mmm$ setting. (b) Waterfall plot across the temperature range studied.

tice symmetry depending on the ordering pattern of the distinct Ti ions in neighboring unit cells. Repeating the symmetry-lowered plaquette uniformly along the a - and b -directions results in no change of the unit cell, but breaks the metric symmetry from C_4 in $P4/mmm$ to C_2 in $Pmmm$, as observed experimentally. This arrangement of charges can be described as an intra-unit-cell nematic CDW. Our data are therefore consistent with the formation of such a CDW on cooling through T_a .

This charge order is energetically favored on Coulombic grounds if the onsite Hubbard energy U is sufficiently small, which is a reasonable assumption since the system is a metal rather than a Mott insulator. The transfer of a charge of δ from $\text{Ti}(1)$ to $\text{Ti}(2)$ will result in a lowering of the electrostatic energy, $V(1-\delta)(1+\delta) = V(1-\delta^2)$, where V is the screened Coulomb interaction between Ti sites and is positive. The result is charge order with a d -wave symmetry³⁹ with the sign of the modulated charge density varying as $-+ -+$ around the plaquette. From plaquette to plaquette, the orientation of the axis of the distortion can be parallel or perpendicular, forming a “ferro-” or “anti-ferro-” type ordering which would preserve or break translational symmetry, respectively. The former is consistent with the experimental observa-

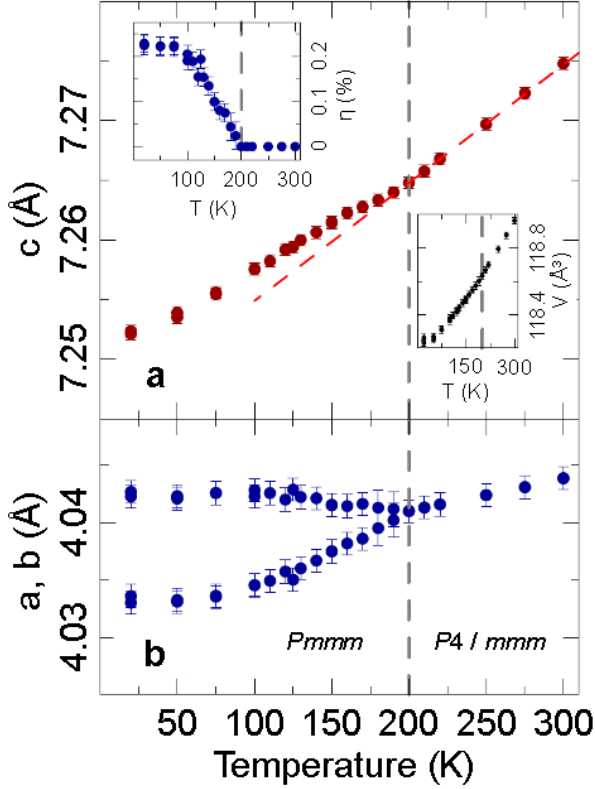


FIG. 4. Temperature evolution of BaTi₂As₂O structural parameters. (a) Lattice parameter *c* (red). (b) Lattice parameters *a*, *b* (blue). Insets: orthorhombicity $\eta = 2 \times (a-b)/(a+b)$ (left) and unit cell volume (right). Vertical dashed gray line indicates transition temperature. Dashed red line is a guide for the eyes.

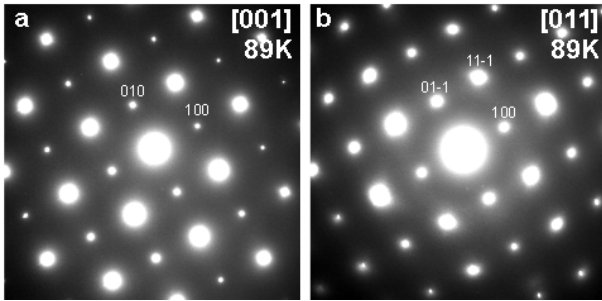


FIG. 5. Electron diffraction patterns of BaTi₂As₂O. (a) Diffraction pattern with the incident beam along the [001] and (b) along the [011] directions. No superlattice peaks are observed at low temperature even after heavy overexposure.

tions in this material. We suggest that the rather rigid face-shared octahedral topology in each layer favors the uniform “ferro-” over the “anti-ferro-” ordering.

This charge-nematic order naturally explains the observed changes in the *a*- and *c*-lattice parameters. The transfer of charge from the Ti(1) $d_{y^2-z^2}$ orbital to the Ti(2) $d_{x^2-z^2}$ results in increased electrostatic repulsion between the charge-rich $d_{x^2-z^2}$ orbitals extending along the *a*-axis, breaking the tetragonal degeneracy of the *a*-

and *b*-axes and leading to the observed orthorhombic distortion. Furthermore, a uniform stacking of the CDWs in each layer can also explain the response of the *c*-axis lattice parameter, which expands upon entering the CDW state (Fig. 4(a)). This lattice expansion may be attributed to increased electrostatic repulsion between inter-layer Ti ions from the transferred charge. The net energy contribution is $V'[(1+\delta)^2 + (1-\delta)^2] = V'(2+2\delta^2)$, where V' is the inter-layer screened Coulomb interaction.

The structural effects observed on cooling are much smaller in BaTi₂Sb₂O than BaTi₂As₂O, suggesting that the CDW is relatively suppressed both in amplitude and temperature. This may be a result of the larger unit cell in the Sb compound, due to its larger Sb³⁻ ionic diameter (2.25 Å vs. 1.98 Å for As³⁻)¹⁸, resulting in a smaller *V*.

To identify the microscopic driving force of this nematic instability, we present a symmetry-based zero-order analysis in which only the leading energy scales are retained. Ti atoms reside at the center of a distorted octahedron with oxygen at the apices and pnictide atoms around the equatorial plane, as shown in Fig. 1(d) for Ti(1). The Ti 3*d*-energy levels are illustrated in Fig. 1(e), similar to the case of nearly isostructural (LaO)₂CoSe₂O⁴⁰. The nominal electron occupation is one electron per Ti atom, which would have been assigned to the locally lowest lying $d_{y^2-z^2}$ and $d_{x^2-z^2}$ orbitals on the Ti(1) and Ti(2) ions, respectively. However, the σ -bonding between the Ti(1) and Ti(2) d_{xy} orbitals forms a relatively wide band that overlaps the locally lowest level. Therefore, the minimum model for the titanium oxypnictides involves the two orbitals: $d_{y^2-z^2}$ and d_{xy} on Ti(1) and $d_{x^2-z^2}$ and d_{xy} on Ti(2). Since the d_{xy} orbital has the same impact on both the *a* and *b* direction, the $C_4 - C_2$ symmetry lowering around the central oxygen atom is mainly determined by the charge imbalance between the quasi-one-dimensional $d_{y^2-z^2}$ band on Ti(1) and $d_{x^2-z^2}$ on Ti(2) as a result of the Stoner instability⁴¹. No doubt this mechanism will be complicated by hybridization and other issues, but this symmetry-based analysis provides the appropriate realistic starting point. Since the proposed intra-unit-cell charge-nematic order elegantly explains all the observed structural effects, it is anticipated to be the electronic ground state of BaTi₂Pn₂O.

Methods

Powder specimens of BaTi₂As₂O and BaTi₂Sb₂O were prepared via conventional solid state reaction methods. Details of the synthesis are provided in a previous study²⁶. Time-of-flight neutron total scattering experiments were performed at the Neutron Powder Diffractometer at Los Alamos Neutron Science Center (LANSCE) at Los Alamos National Laboratory. Data were collected using a closed-cycle He refrigerator at temperatures ranging from 10 - 300 K in steps of 10 K near the CDW transition and 25 K away from the transition over a wide range of momentum transfer *Q*. Le Bail³⁸ fits to the intensity profiles were performed with GSAS⁴² on the EXPGUI platform⁴³. Pair distribution function

(PDF) profiles were obtained by Fourier transforming the measured total scattering intensity up to a maximum momentum transfer of $Q_{max} = 24 \text{ \AA}^{-1}$ using established protocols^{44,45} as implemented in the program PDFgetN⁴⁶. The Le Bail fits were used to extract lattice parameters and space group symmetry, the PDF fits to extract atomic displacement parameters. Symmetry mode analysis using the program ISODISTORT⁴⁷ was conducted to identify candidate distorted structures. Electron diffraction patterns were recorded using a JEOL ARM 200CF transmission electron microscope (TEM), operated at 200 keV, at Brookhaven National Laboratory. The TEM samples were prepared by crushing powder specimens into thin flakes transparent to the electron beam, which were supported by a lacey carbon copper grid. DFT calculations were performed within the generalized gradient approximation (GGA) implemented in the Wien2k software package⁴⁸.

Acknowledgements

X-ray and electron diffraction work at Brookhaven National Laboratory were supported by the U.S. Department of Energy, Office of Basic Energy Sciences, under contract No. DE-AC02-98CH10886. BF at Columbia were supported by the U.S. National Science Founda-

tion (NSF) through grant OISE-0968226. The work at Kyoto University was supported by the FIRST program, Japan Society of the Promotion of Science (JSPS). YJU was supported by NSF DMR-1105961, the Japan Atomic Energy Agency Reimei project, and the Friends of To-dai Inc. Neutron scattering experiments were carried out on NPDF at LANSCE, funded by DOE Office of Basic Energy Sciences LANL is operated by Los Alamos National Security LLC under DOE Contract No. DE-AC52-06NA25396.

Author contributions

YU, SB, and BF initiated this work. YN and HK carried out sample preparation and characterization. EB carried out the neutron diffraction measurements and analysed the data with assistance from BF. HH performed the electron diffraction measurements with help from YZ. WY proposed the charge-ordering model and provided theoretical support. BF, WY, and SB wrote the paper, with input from all authors.

Additional information

Supplementary information is available in the online version of the paper. Correspondence should be addressed to S.J.L.B.

Competing financial interests

The authors declare no competing financial interests.

* These authors contributed equally to this work.

† sb2896@columbia.edu

¹ Dagotto, E. *et al.* *Nanoscale phase separation and colossal magnetoresistance* (Springer-Verlag, Amsterdam, 2003).

² Dagotto, E. Complexity in strongly correlated electronic systems. *Science* **309**, 257–262 (2005).

³ Orenstein, J. & Millis, A. J. Advances in the physics of high-temperature superconductivity. *Science* **288**, 468–474 (2000).

⁴ da Silva Neto, E. H. *et al.* Ubiquitous interplay between charge ordering and high-temperature superconductivity in cuprates. *Science* **343**, 393 (2014).

⁵ Fernandes, R., Chubukov, A. & Schmalian, J. What drives nematic order in iron-based superconductors? *Nat. Phys.* **10**, 97 (2014).

⁶ Tranquada, J. M., Sternlieb, B. J., Axe, J. D., Nakamura, Y. & Uchida, S. Evidence for stripe correlations of spins and holes in copper oxide superconductors. *Nature* **375**, 561 (1995).

⁷ Hoffman, J. E. *et al.* A four unit cell periodic pattern of quasi-particle states surrounding vortex cores in $\text{Bi}_2\text{Sr}_2\text{CaCu}_2\text{O}_{8+\delta}$. *Science* **295**, 466–469 (2002).

⁸ Vershinin, M. *et al.* Local ordering in the pseudogap state of the high- T_c superconductor $\text{Bi}_2\text{Sr}_2\text{CaCu}_2\text{O}_{8+\delta}$. *Science* **303**, 1995–1998 (2004).

⁹ Chang, J. *et al.* Direct observation of competition between superconductivity and charge density wave order in $\text{YBa}_2\text{Cu}_3\text{O}_{6.67}$. *Nat. Phys.* **8**, 871–876 (2012).

¹⁰ Comin, R. *et al.* Charge order driven by fermi-arc instability in $\text{Bi}_2\text{Sr}_{2-x}\text{La}_x\text{CuO}_{6+\delta}$. *Science* **343**, 390 (2014).

¹¹ Lawler, M. J. *et al.* Intra-unit-cell nematicity of the high- T_c copper-oxide pseudogap states. *Nature* **466**, 374–377 (2010).

¹² Varma, C. Non-Fermi-liquid states and pairing instability

of a general model of copper oxide metals. *Phys. Rev. B* **55**, 14554 (1997).

¹³ Li, Y. *et al.* Hidden magnetic excitation in the pseudogap phase of a high- t_c superconductor. *Nature* **468**, 283 (2010).

¹⁴ Chuang, T. *et al.* Nematic electronic structure in the “parent” state of the iron-based superconductor $\text{Ca}(\text{Fe}_{1-x}\text{Co}_x)_2\text{As}_2$. *Science* **327**, 181–184 (2010).

¹⁵ Lee, P. A., Nagaosa, N. & Wen, X.-G. Doping a mott insulator: Physics of high-temperature superconductivity. *Rev. Mod. Phys.* **78**, 17–85 (2006).

¹⁶ Fernandes, R., Chubukov, A., Knolle, J., Eremin, I. & Schmalian, J. Preemptive nematic order, pseudogap, and orbital order in the iron pnictides. *Phys. Rev. B* **85**, 024534 (2012).

¹⁷ Yajima, T. *et al.* Synthesis and physical properties of the new oxybismuthides $\text{BaTi}_2\text{Bi}_2\text{O}$ and $(\text{SrF})_2\text{Ti}_2\text{Bi}_2\text{O}$ with a d^1 square net. *J. Phys. Soc. Jpn.* **82**, 013703 (2013).

¹⁸ Yajima, T. *et al.* Two superconducting phases in the iso-valent solid solutions $\text{BaTi}_2\text{Pn}_2\text{O}$ ($\text{Pn} = \text{As}, \text{Sb}, \text{and Bi}$). *J. Phys. Soc. Jpn.* **82**, 033705 (2013).

¹⁹ Zhai, H.-F. *et al.* Superconductivity, charge- or spin-density wave, and metal-nonmetal transition in $\text{BaTi}_2(\text{Sb}_{1-x}\text{Bi}_x)_2\text{O}$. *Phys. Rev. B* **87**, 100502 (2013).

²⁰ Ozawa, T. C. & Kauzlarich, S. M. Chemistry of layered d-metal pnictide oxides and their potential as candidates for new superconductors. *Sci. Technol. Adv. Mater.* **9**, 033003 (2008).

²¹ Wang, X. F. *et al.* Structure and physical properties for a new layered pnictide-oxide: $\text{BaTi}_2\text{As}_2\text{O}$. *J. Phys: Condens. Mat.* **22**, 075702 (2010).

²² Liu, R. H. *et al.* Structure and physical properties of the layered pnictide-oxides: $(\text{SrF})_2\text{Ti}_2\text{Pn}_2\text{O}$ ($\text{Pn} = \text{As}, \text{Sb}$) and $(\text{SmO})_2\text{Ti}_2\text{Sb}_2\text{O}$. *Chemistry of Materials* **22**, 1503–

- 1508 (2010).
- ²³ Johrendt, D., Hosono, H., Hoffmann, R.-D. & Pöttgen, R. Structural chemistry of superconducting pnictides and pnictide oxides with layered structures. *Z. Kristallogr.* **226**, 435–446 (2011).
 - ²⁴ Yajima, T. *et al.* Superconductivity in $\text{BaTi}_2\text{Sb}_2\text{O}$ with a d^1 square lattice. *J. Phys. Soc. Jpn.* **81**, 103706 (2012).
 - ²⁵ Doan, P. *et al.* $\text{Ba}_{1-x}\text{Na}_x\text{Ti}_2\text{Sb}_2\text{O}$ ($0.0 \leq x \leq 0.33$): A layered titanium-based pnictide oxide superconductor. *J. Am. Chem. Soc.* **134**, 16520–16523 (2012).
 - ²⁶ Nozaki, Y. *et al.* Muon spin relaxation and electron/neutron diffraction studies of $\text{BaTi}_2(\text{As}_{1-x}\text{Sb}_x)_2\text{O}$: Absence of static magnetism and superlattice reflections. *Phys. Rev. B* **88**, 214506 (2013).
 - ²⁷ von Rohr, F., Schilling, A., Nesper, R., Baines, C. & Bendele, M. Conventional superconductivity and charge-density-wave ordering in $\text{Ba}_{1-x}\text{Na}_x\text{Ti}_2\text{Sb}_2\text{O}$. *Phys. Rev. B* **88**, 140501 (2013).
 - ²⁸ Gooch, M. *et al.* Weak coupling BCS-like superconductivity in the pnictide oxide $\text{Ba}_{1-x}\text{Na}_x\text{Ti}_2\text{Sb}_2\text{O}$ ($x = 0$ and 0.15). *Phys. Rev. B* **88**, 064510 (2013).
 - ²⁹ III, E. A., Ozawa, T., Kauzlarich, S. M. & Singh, R. R. Phase transition and spin-gap behavior in a layered tetragonal pnictide oxide. *J. Solid State Chem.* **134**, 423 – 426 (1997).
 - ³⁰ Liu, R. H. *et al.* Physical properties of the layered pnictide oxides $\text{Na}_2\text{Ti}_2\text{p}_2\text{O}$ ($p=\text{As}, \text{Sb}$). *Phys. Rev. B* **80**, 144516 (2009).
 - ³¹ Kitagawa, S., Ishida, K., Nakano, K., Yajima, T. & Kageyama, H. s -wave superconductivity in superconducting $\text{BaTi}_2\text{Sb}_2\text{O}$ revealed by $^{121/123}\text{Sb}$ -NMR/nuclear quadrupole resonance measurements. *Phys. Rev. B* **87**, 060510 (2013).
 - ³² Singh, D. J. Electronic structure, disconnected fermi surfaces and antiferromagnetism in the layered pnictide superconductor $\text{Na}_x\text{Ba}_{1-x}\text{Ti}_2\text{Sb}_2\text{O}$. *New J. Phys.* **14**, 123003 (2012).
 - ³³ Wang, G., Zhang, H., Zhang, L. & Liu, C. The electronic structure and magnetism of $\text{BaTi}_2\text{Sb}_2\text{O}$. *J. Appl. Phys.* **113** (2013).
 - ³⁴ Subedi, A. Electron-phonon superconductivity and charge density wave instability in the layered titanium-based pnictide $\text{BaTi}_2\text{Sb}_2\text{O}$. *Phys. Rev. B* **87**, 054506 (2013).
 - ³⁵ Xu, H. C. *et al.* Electronic structure of the $\text{BaTi}_2\text{As}_2\text{O}$ parent compound of the titanium-based oxypnictide superconductor. *Phys. Rev. B* **89**, 155108 (2014).
 - URL <http://link.aps.org/doi/10.1103/PhysRevB.89.155108>.
 - ³⁶ Abeykoon, M. *et al.* Evidence for short-range-ordered charge stripes far above the charge-ordering transition in $\text{La}_{1.67}\text{Sr}_{0.33}\text{NiO}_4$. *Phys. Rev. Lett.* **111**, 096404 (2013).
 - ³⁷ Božin, E. S., Billinge, S. J. L., Takagi, H. & Kwei, G. H. Neutron diffraction evidence of microscopic charge inhomogeneities in the CuO_2 plane of superconducting $\text{La}_{2-x}\text{Sr}_x\text{Cu}_4$ ($0 \leq x \leq 0.30$). *Phys. Rev. Lett.* **84**, 5856–5859 (2000).
 - ³⁸ Le Bail, A., Duroy, H. & Fourquet, J. L. Ab-initio structure determination of LiSbWO_6 by x-ray powder diffraction. *Mater. Res. Bull.* **23**, 447–452 (1987).
 - ³⁹ Comin, R. *et al.* The symmetry of charge order in cuprates. *Arxiv* **1402.5415** (2014).
 - ⁴⁰ Wu, H. Electronic structure, spin state, and magnetism of the square-lattice mott insulator $\text{LaCo}_2\text{Se}_2\text{O}_3$ from first principles. *Phys. Rev. B* **82**, 020410(R) (2010).
 - ⁴¹ Fischer, M. H. & Kim, E.-A. Mean-field analysis of intra-unit-cell order in the Emery model of the CuO_2 plane. *Phys. Rev. B* **84**, 144502 (2011).
 - ⁴² Larson, A. C. & Von Dreele, R. B. General structure analysis system (1994). Report No. LAUR-86-748, Los Alamos National Laboratory, Los Alamos, NM 87545.
 - ⁴³ Toby, B. H. EXPGUI, a graphical user interface for GSAS. *J. Appl. Crystallogr.* **34**, 201–213 (2001).
 - ⁴⁴ Egami, T. & Billinge, S. J. L. *Underneath the Bragg peaks: structural analysis of complex materials* (Elsevier, Amsterdam, 2012), 2nd edn.
 - ⁴⁵ Chupas, P. J. *et al.* Rapid acquisition pair distribution function analysis (RA-PDF). *J. Appl. Crystallogr.* **36**, 1342–1347 (2003).
 - ⁴⁶ Peterson, P. F., Gutmann, M., Proffen, T. & Billinge, S. J. L. PDFgetN: a user-friendly program to extract the total scattering structure function and the pair distribution function from neutron powder diffraction data. *J. Appl. Crystallogr.* **33**, 1192–1192 (2000).
 - ⁴⁷ Campbell, B., Stokes, H., Tanner, D. & Hatch, D. ISODISPLACE: An Internet Tool for Exploring Structural Distortions. *J. Appl. Crystallogr.* **39**, 607–614 (2006).
 - ⁴⁸ Blaha, P., Schwarz, K., Madsen, G., Kvasnicka, d. & Luitz, J. *WIEN2k: An Augmented Plane Wave Plus Local Orbitals Program for Calculating Crystal Properties*. Vienna University of Technology, Inst. of Physical and Theoretical Chemistry (2001).

Intra-unit-cell nematic charge order in the titanium-oxypnictide family of superconductors: Supplementary Information

Benjamin A. Frandsen¹, Emil S. Bozin², Hefei Hu², Yimei Zhu², Yasumasa Nozaki³, Hiroshi Kageyama³, Yasutomo J. Uemura¹, Wei-Guo Yin², and Simon J. L. Billinge^{2,4}

¹ Department of Physics, Columbia University, New York, NY 10027, USA

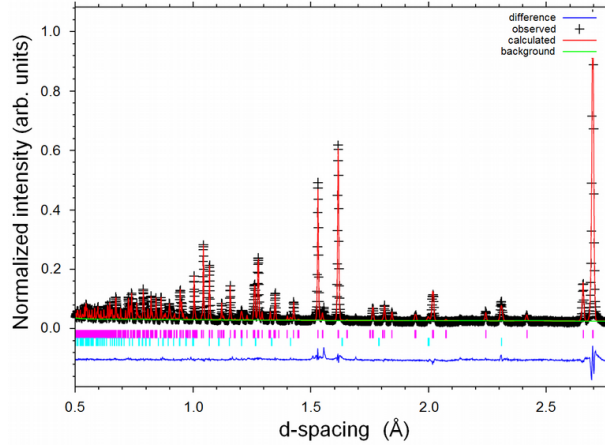
² Condensed Matter and Materials Science Department, Brookhaven National Laboratory, Upton, NY 11973, USA

³ Department of Energy and Hydrocarbon Chemistry, Graduate School of Engineering, Kyoto University, Nishikyo, Kyoto 615-8510, Japan

⁴ Department of Applied Physics and Applied Mathematics, Columbia University, New York, NY 10027, USA

1. Rietveld refinement of BaTi₂As₂O

Rietveld refinement of BaTi₂As₂O at 20 K was carried out using the *Pmmm* model (Sup. Fig. 1). A small number of weak impurity peaks have been observed, and well explained as belonging to a BaTiO₃ impurity phase on the level of 2.6(1)% weighted fraction. Fit residuals were $R_{wp} = 0.041$ and $R_p = 0.025$. The orthorhombic lattice parameters refined to $a = 4.0423(5)\text{\AA}$, $b = 4.0327(5)\text{\AA}$, and $c = 7.2523(3)\text{\AA}$. Additional refined parameters are provided in Table 1.



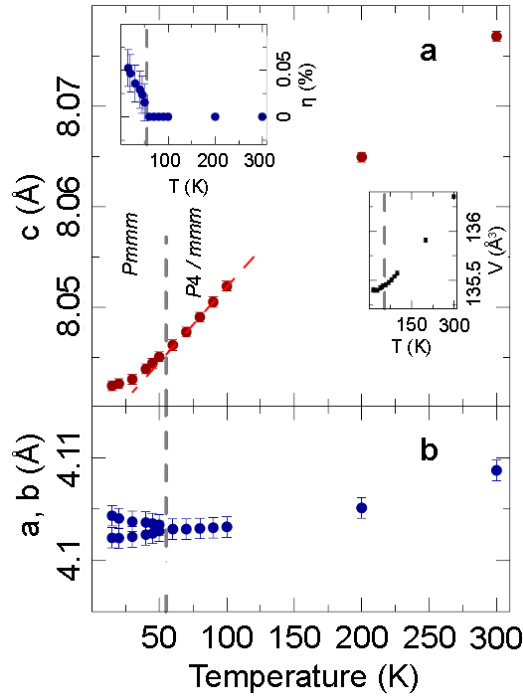
Sup. Fig. 1: Rietveld structure refinement of BaTi₂As₂O data at 20 K using *Pmmm* model. Principal phase reflections are shown as purple tickmarks, those of BaTiO₃ impurity phase as blue tickmarks. Weighted fraction of the impurity phase was found to be 2.6(1)%.

Table 1: Atomic parameters of BaTi₂As₂O

Atom	Wyckoff site	x	y	z	U_{iso} (Å ²)
Ba	1h	0.500000	0.500000	0.500000	0.0023(3)
Ti	1e	0.000000	0.500000	0.000000	0.0040(6)
Ti	1b	0.500000	0.000000	0.000000	0.0045(6)
As	2q	0.000000	0.000000	0.7559(1)	0.0035(2)
O	1f	0.500000	0.500000	0.000000	0.0058(3)

2. Structural refinement of BaTi₂Sb₂O

Le Bail refinements of the BaTi₂Sb₂O diffraction patterns for all measured temperatures were conducted. The undistorted *P4/mmm* model can be used with moderate success at all temperatures, but the distorted *Pmmm* model yields a better fit below 50 K, coinciding with T_a . Sup. Fig. 2 displays the results of the Le Bail refinements using *P4/mmm* for $T \geq 50$ K and *Pmmm* for $T < 50$ K. As with BaTi₂As₂O, orthorhombic splitting of the *a*-axis and a slight upturn in the *c*-axis parameter are observed, but the magnitude of these distortions is reduced by a



Sup. Fig. 2: Results of Le Bail refinement for $\text{BaTi}_2\text{Sb}_2\text{O}$. (a) Temperature dependence of the c -axis. Insets: orthorhombicity $\eta = 2 \times (a - b)/(a + b)$ (left) and unit cell volume (right). (b) Temperature dependence of the a and b axes, showing a small orthorhombic splitting below $T \sim 50$ K.

factor of ~ 5 compared to $\text{BaTi}_2\text{As}_2\text{O}$. These results demonstrate that the observed structural response tracks closely with the CDW transition, with the magnitude of the structural distortions proportional to the CDW transition temperature. These results also agree with and explain the anomalous behavior of $P4/mmm$ lattice parameters reported in Fig. 2 of Ref. [1].

3. Pair distribution function and atomic displacement parameters

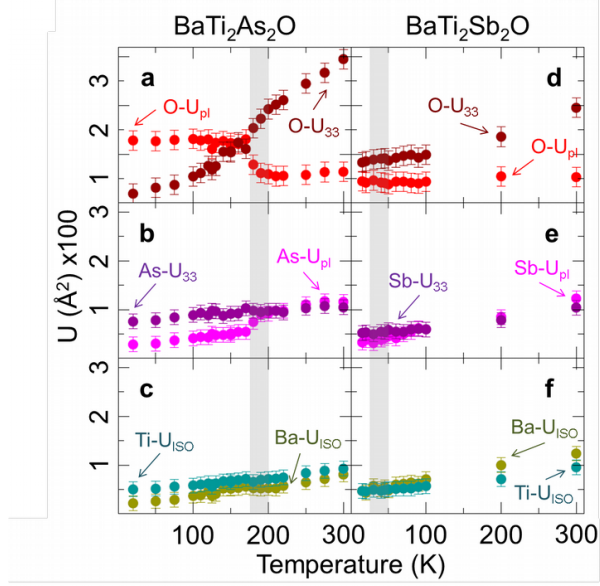
Pair distribution function (PDF) refinements were conducted for both $\text{BaTi}_2\text{As}_2\text{O}$ and $\text{BaTi}_2\text{Sb}_2\text{O}$ to extract atomic displacement parameters (ADPs). PDF analysis allows more reliable extraction of ADPs than conventional Rietveld refinements when the signal-to-noise ratio at high momentum transfer is suboptimal [2], as was the case for our measurements. Only in the case of $\text{BaTi}_2\text{As}_2\text{O}$ at 20 K were the data of high enough quality for reliable Rietveld refinement of ADPs.

The results of a fit of the tetragonal $P4/mmm$ model to the PDFs at all temperatures for both compounds are displayed in Sup. Fig. 3. The most noticeable feature is the pronounced change in the oxygen in-plane (U_{pl}) and out-of-plane (U_{33}) ADPs around 200 K for $\text{BaTi}_2\text{As}_2\text{O}$, qualitatively verifying the occurrence of a phase transition at this temperature. The large increase in the oxygen U_{pl} as the temperature is lowered through T_a indicates the appearance of a distribution of O-Ti bond lengths, consistent with the orthorhombic distortion that lowers the C_4 symmetry of the O-site to C_2 and results in two distinct O-Ti distances. The ADPs of the other atoms in $\text{BaTi}_2\text{As}_2\text{O}$ show a smaller response to the transition. The effects in $\text{BaTi}_2\text{Sb}_2\text{O}$ fall within the error bars.

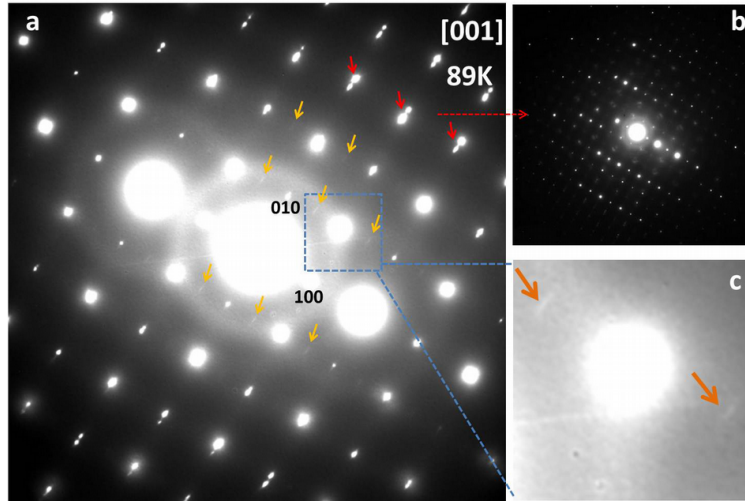
4. Electron diffraction superlattice peaks near grain boundaries

Electron diffraction measurements of $\text{BaTi}_2\text{As}_2\text{O}$ showed no superlattice peaks for the vast majority of the areas of the sample surveyed, pointing to the uniform $\mathbf{Q} = 0$ configuration, as discussed in the text. However, a few areas in the immediate vicinity of grain boundaries displayed low-temperature weak superlattice peaks with $\mathbf{Q} = (1/2, 0, 0)$ or $\mathbf{Q} = (0, 1/2, 0)$. Some areas near a grain boundary had both types of superlattice reflections superimposed. A representative diffraction pattern from a grain boundary area is displayed in Sup. Fig. 4. The superlattice peaks disappeared at high temperature.

It is interesting to consider how the appearance of these superlattice peaks near grain boundaries relates to the



Sup. Fig. 3: Results of PDF refinements of in-plane (U_{pl}), out-of-plane (U_{33}), and isotropic (U_{iso}) atomic displacement parameters of O, As, Ba, and Ti for the $P4/mmm$ model of $BaTi_2As_2O$ and $BaTi_2Sb_2O$.



Sup. Fig. 4: (a) Electron diffraction pattern showing superlattice peaks (indicated by yellow arrows) with $Q = (1/2, 0, 0)$. Red arrows indicate the split Bragg peaks associated with the grain boundary. (b) Diffraction pattern with a larger field of view showing two sets of reflections arising from the grain boundary. (c) Magnified view of two superlattice peaks.

proposed d -wave CDW discussed in the main text. The intra-unit-cell CDW could in principle arrange itself in a variety of ordering configurations in the ab -plane. For example, a $\mathbf{Q} = 0$ ordering results from a single plaquette being repeated uniformly along both the a - and b -directions, as introduced in the main text. A second possibility involves a 90° rotation of successive plaquettes along one direction but uniform translation along the other, resulting in a doubling of the unit cell with $\mathbf{Q} = (1/2, 0, 0)$ or $\mathbf{Q} = (0, 1/2, 0)$. A third possibility arises from this 90° modulation acting in both planar directions, resulting in a checkerboard pattern with $\mathbf{Q} = (1/2, 1/2, 0)$ that would preserve overall tetragonal symmetry. Since superlattice peaks of the $\mathbf{Q} = (1/2, 0, 0)$ type are observed near grain boundaries, we suggest that the strain field induced by the grain boundary favors a 90° rotation of the CDW orientation, most likely in the direction perpendicular to the grain boundary, while no such modulation occurs in the orthogonal direction. Further studies are required to verify this interpretation of these superlattice peaks.

References

- [1] Yajima, T. *et al.* Superconductivity in $\text{BaTi}_2\text{Sb}_2\text{O}$ with a d^1 square lattice. *J. Phys. Soc. Jpn.* **81**, 103706 (2012).
- [2] Egami, T. & Billinge, S. J. L. *Underneath the Bragg peaks: structural analysis of complex materials* (Elsevier, Amsterdam, 2012), 2nd edn.